Formation of Turbulence on a Tilted Density Interface

by

Carl H. Gibson[1] and Jörg Imberger[2]

[1]University of California at San Diego, La Jolla, CA 92093-0411

[2]University of Western Australia, Nedlands, Western Australia 6009

Abstract

Turbulence formation in Kelvin-Helmholtz (KH) billows on a thin, tilted, density interface is examined by analytical modeling and the model is compared to laboratory tilt tube experiments. Previously, from dye and shadowgraph billow patterns and because the KH instability is inviscid, such experiments have been interpreted as an inviscid roll-up of the density-vorticity interface to maximum size, followed by gravitational collapse of the billow to form smaller scale turbulence and maximum viscous and scalar dissipation rates ε and χ. The present "turbulent KH billow" model suggests that internal wave breaking stages in the laboratory, ocean, or atmosphere are not inviscid but the opposite. The first eddies appear at viscous (Kolmogorov) scales and these grow by entrainment, as usual for turbulence formation, either in the two accelerating boundary layers of the tilted density interface or in the strongly sheared "braid" layers that develop on either side of a billow just prior to its appearance. The scale of the initial roll-up for a thin interface is determined by the thickness of these boundary layers when their interface Froude numbers exceed a critical value. Energy (Obukhov) scales of the turbulence are initially constrained by strong Coriolis forces in the radial direction of the billows due to their spin, but ε is enhanced by vortex stretching in both the billows and braids, so that ε and χ are maximum, not minimum, in the early stages of billow growth, and there is no gravitational collapse of the fossil turbulence remnants. Turbulent braid layers thicken by entrainment, wrap around the billows, and eventually scramble the organized billow structure and destroy its false inviscid appearance when the intensified turbulence overcomes the Coriolis constraints. The turbulent billows pair to form larger billows and the resulting fully turbulent shear layer grows unaffected by gravity until the large eddy inertial forces are balanced by buoyancy forces and the conversion of the velocity and density fields to fossil turbulence internal waves and microstructure begins.

1. Introduction

Turbulence and mixing in the interior of the atmosphere and ocean is both a result and source of internal waves, a consequence of their breaking and a mechanism of their generation. Considerable uncertainty exists concerning the detailed nature of the internal wave and turbulence formation processes. How to distinguish between internal waves and turbulence, and how they are coupled in mixing and diffusion processes are open questions. It is important to identify and interpret signatures of "wave breaking", "turbulence", or "fossil turbulence" that appear as overturns and microstructure of normally stratified fields such as temperature, humidity, salinity, refractive index, or density. Although the most numerous such mixing events will be at small vertical scales on weak gradients, the events that dominate the vertical mixing must be rare and powerful, and must

occur with large vertical overturning scales on those surfaces with maximum density gradients; that is, on the strongest pycnoclines. Otherwise the weaker gradients between such surfaces would be mixed away, leaving progressively fewer and stronger pycnoclines, but this is not observed. In this paper we examine laboratory observations of waves and turbulence forming on tilted density interfaces to reinterpret recent oceanic observations of rare, large scale density overturning events. Can such overturns occur without previous, powerful turbulence? We first must define turbulence and distinguish it from nonlinear "wave" motions dominated by viscous, buoyancy, or Coriolis forces. When such wave motions are remnants of previous turbulence events, they have unique properties and signatures and are classified as forms of fossil turbulence. In this Section a brief summary of ocean turbulence and mixing processes is given. Turbulence is defined, and the laboratory evidence and the "inviscid" versus "turbulent" Kelvin-Helmholtz (KH) billow models that have been inferred are contrasted. In Section 2 a theoretical treatment of tilt tube experiments is presented that supports the latter model. Section 3 summarizes the results and conclusions.

Oceanic turbulence and mixing processes

In the ocean, powerful mixing occurs from storms near the upper surface and from strong currents over sills and around islands and seamounts near the bottom, producing strong pycnoclines at boundaries of the resulting mixed layers. These pycnoclines are eroded back toward the original uniform vertical density gradient by a cascade of smaller and less powerful mixing events. The strongest pycnoclines of interior stratified layers of the atmosphere and ocean appear to be associated with horizontal fronts due to horizontal stirring on scales limited by planetary Coriolis forces, Gibson (1990, 1991abd). Therefore these interior pycnoclines are separated by scales comparable to the size of the largest horizontal turbulent eddies, which may be tens or hundreds of kilometers. Persistent tilting of such frontal pycnoclines from the horizontal stirring will result in the buildup of thick shear layers that temporarily strengthen the pycnoclines and inhibit both turbulence and waves on these layers, but will eventually lead to powerful turbulence events that dissipate the stored kinetic energy near the density interfaces and locally break up the strong pycnolines into intermediate scale steps. Consequently, turbulence and mixing in the eddy-diffusion-flux layers of the ocean and atmosphere are extremely intermittent in space and time, with large decorrelation length and time scales, Gibson (1991c). Control volumes surrounding such layers must be larger than the largest eddy sizes of their dominant horizontal and vertical turbulence events, Gibson (1990, 1991c), for the concept of turbulent eddy diffusion to have physical significance, and these sizes are determined by buoyancy forces in the vertical, Coriolis forces in the horizontal, and the strength of the turbulence events as measured by their viscous dissipation rates ε. In order to estimate average turbulence and mixing rates from oceanic microstructure measurements, it is important to be able to recognize and distinguish between the signatures of turbulence, fossil turbulence, and internal wave breaking events. Fossil turbulence models have been developed by Gibson (1980), and Imberger and Ivey (1991) that focus on these distinctions and classify microstructure using hydrodynamic phase diagrams according to hydrodynamic state.

Turbulence is caused by shear instability arising from the nonlinear term $\mathbf{v} \times \omega$ in the momentum equations (equation (4) in Section 2.1); that is, the inertial-vortex force per unit mass, where $\mathbf{v}$ is velocity and ω is vorticity. Inertial vortex forces amplify perturbations of shear layers and cause such vortex sheets to roll up into eddies on all scales not inhibited by viscous, buoyancy,

Coriolis, or other forces. Generally, the small scale eddies form first because their overturn times are smaller. The overturn time for an eddy of scale L to form will depend on the perturbation velocity V at this scale normal to the shear layer. In turbulence $V \approx (\varepsilon L)^{1/3}$, so overturn times τ increase with size because $\tau \approx L/V \approx L^{2/3}$. These eddies pair, and a cascade of pairings and entrainment leads to turbulence up to the largest scales permitted by the constraining forces (the Ozmidov or Hopfinger scales) or the fluid boundaries. In discussions of turbulence, and in some theoretical models such as Lumley (1992), it is often assumed that large eddies form first and these break down sequentially into smaller and smaller scale eddies. However, actual turbulent flows generally fail to show this behavior unless a strong perturbation velocity is imposed artificially, such as by flapping the splitter plate for a shear flow. Even here, the smaller eddies will form on the rolled up vortex sheet and rapidly fill the spectral gap between the imposed and the more rapidly growing eddies originating at Kolmogorov scale wavenumbers.

From the conservation of vorticity equation (equation (2) in Section 2.1), vorticity in a stratified fluid is produced at a rate $(\nabla\rho\times\nabla p)/\rho^2$. Thus, shear kinetic energy will accumulate on surfaces with the maximum density gradients, just where turbulence formation is most strongly inhibited. The pressure gradient ∇p in the interior of a stratified fluid is nearly constant and downward, with $\nabla p = -\rho g\mathbf{k}$, where $\mathbf{k}$ is the upward unit vector, so for random surface tilting independent of $\nabla\rho$, the rate of vorticity production is proportional to the magnitude of the density gradient. The total amount of kinetic energy accumulated at a particular tilted pycnocline increases as the square of the time it is tilted. The stronger the density gradient, the longer it can persist before it is broken up by turbulence. Once turbulence begins and grows, most of the accumulated kinetic energy in the shear layer will be rapidly absorbed and dissipated by the event, and the largest turbulence scales will be rapidly damped by buoyancy, leaving remnant partially mixed microstructure patches as fossils of the previous turbulence. The resulting strong pycnoclines bounding the fossils are eroded back toward a uniform vertical gradient by a sequence of progressively smaller and smaller strength parasitic turbulent events, producing smaller and smaller step structures in a "fossil turbulence cascade", Gibson (1987a). In addition, forced internal waves with the amplitude of the largest turbulent eddy will emanate from the billow turbulence events, Gibson (1991c). These can trigger other turbulence events and greatly expand the volume of stratified fluid influenced by the primary turbulence event. Because these waves preserve information about the strength and age of the primary turbulence event that produced them, they are termed "fossil turbulence internal waves" by Gibson (1991c).

Since the actual transition to turbulence in stratified flows is so localized in space and time, conventional inviscid stability theories involving the relative growth rates of Fourier modes are not very useful in transition analysis without including a large amount of phase information, and may be misleading with respect to dissipation signatures of stratified turbulence events, and the scales at which turbulence will first appear. In this paper, turbulence is defined as an eddy-like state of fluid motion where the inertial-vortex forces of the eddies are larger than any other forces that may tend to damp them out, Gibson (1991e). By this definition, all motions dominated by buoyancy or Coriolis forces are nonturbulent even though they are random and have nonlinear dynamics, and all irrotational flows are nonturbulent, even those that are eddy-like. The random spiral flow of irrotational fluid as it is entrained by turbulence is not turbulence. Internal waves and Coriolis eddies caused by turbulence are forms of fossil vorticity turbulence, following the terminology of

the Gibson (1980, 1986, 1991a) fossil turbulence theory. Such motions are treated as turbulence in many oceanographic publications about random microstructure and mesostructure. However, such waves and eddies have different properties than turbulence: they decay slowly, they do not entrain, and their energy spectra are more concentrated at large scales (redder). Fossil turbulence is defined as any fluctuation in a flow or scalar field produced by turbulence that persists after the fluid is no longer turbulent at the scale of the fluctuation, Gibson (1980). Most temperature and salinity microstructure measured in the ocean appears to be fossil turbulence at the largest scales with embedded smaller scale active turbulence; that is, active-fossil turbulence. Most small scale oceanic internal wave motions and Coriolis-inertial eddies also appear to have turbulence origins and therefore may be considered as forms of fossil turbulence.

Inviscid versus turbulent Kelvin-Helmholtz billow models

The tilt tank experiments of Thorpe (1968, 1969, 1971, 1973, 1978, 1987) are often cited as representative of the internal wave breaking process of the ocean interior, and have been used to guide the interpretation of oceanic microstructure signatures, Gregg (1987). In these well known experiments, two initially quiescent water layers of different density and dye color in a transparent rectangular tube are suddenly tilted. The two density layers float up and sink down with equal and opposite accelerations, sometimes to a prescribed velocity limit at tilt back. After a few seconds a series of roll structures appear on the density interface. These grow and eventually break up into a turbulent shear layer. The roll formation is attributed to Kelvin-Helmholtz instability, which is an inviscid process; for example, Van Dyke (1982, plates 145, 146), and Turner (1973, Fig. 4.10, 4.12). From this, and from the organized appearance of the billow structures presented by Thorpe (1971, 1987), Gregg (1987) assumes that oceanic internal wave breaking manifested by Kelvin-Helmholtz billows is inviscid with $\varepsilon \approx 0$. Turbulence with maximum ε is assumed to occur later, by gravitational collapse, after the billow has rolled up to its maximum vertical extent, and after all vertical overturn scales have substantially decreased due to the presumed gravitational collapse. During the hypothetical gravitational collapse the maximum turbulence and density overturn scales are proportional to each other: they both collapse and vanish without a trace. No fossil turbulence microstructure is ever formed in the Gregg (1987) model. Actually, no evidence exists that microstructure overturn scales undergo significant gravitational collapse in laboratory experiments or elsewhere. Overturn scales usually grow somewhat or remain constant, as shown by Gibson (1987b, 1991a), and as discussed in the following Section 2. The persistent of large microstructure overturn scales with $\varepsilon \rightarrow 0$ is the signature of fossil turbulence, and fossil turbulence is what remains after the tilt tube billows according to Thorpe (1973, p748).

This Gregg (1987) "inviscid KH billow model" appears to be a misinterpretation of the laboratory observations as discussed below, and is contrary to their original interpretation by Thorpe. Unfortunately, this model is applied to interpret ocean microstructure data by Moum et al. (1989), Moum et al. (1992), Wijesekera and Dillon (1991), and Hebert et al. (1992). These authors report rare microstructure patches with 20-30 m vertical density overturns, but with ε values much less than expected if the patches were active turbulence, in the strongly sheared and strongly stratified layer above the Pacific equatorial undercurrent high velocity core. The small dissipation rates were used to interpret the patches as the early stages of inviscidly breaking internal waves rather than as active-fossil turbulence patches in advanced states of decay. By means of a fossil

turbulence interpretation, such patches imply previous ε values 10^6-10^7 times larger than the minimum required for stratified turbulence $\varepsilon_F = 30\nu N^2$, Gibson (1980), where ν is the kinematic viscosity and N is the ambient Väisälä frequency. Measured ε values were 10^{-2} to 10^{-5} times smaller than $\varepsilon_0 \approx 3L_T^2N^3$, from an expression for ε_0 of Gibson (1987b), where L_T is the maximum vertical overturn scale, and ε_0 is the dissipation rate at the buoyant-inertial transition where fossilization of active turbulence begins, as discussed in Gibson (1991c).

Reexamination of the Thorpe experiments, and similar new experiments presented in Section 2, show that maximum ε and turbulence appear at early stages of the KH billow formation, well before the maximum overturn scale of the event is achieved, contrary to the Gregg (1987) model. Breaking internal waves in the ocean and atmosphere should also be turbulent, with maximum dissipation rates that occur well before the maximum overturning scales. The probability of any large scale inviscid internal wave breaking in the ocean interior would seem to be small.

Although ε (defined by equation (5) in Section 2.1) was not measured in the initial billow formation stage of the Thorpe experiments, it has sometimes been assumed to be small and the flow nonturbulent because the dye interface between density layers remains relatively unmixed for a few overturnings of the rolls before being scrambled by obvious turbulence, and because the pattern of the overturns is geometrically similar to the inviscid Kelvin-Helmholtz roll-up of a vortex sheet; for example, Rosenhead (1931). Various turbulence formation sequences have been proposed. Thorpe (1987, p5235) states that turbulence begins by some undetermined mechanism during the KH billow formation process, but not later (and suggests that there is agreement about this):

> *"the mechanism leading to three-dimensional motions and turbulence in the billows (and there is agreement that it is here that turbulence first occurs) has not been determined".*

Gregg (1987, Fig. 45, p5283), however, assumes: 1. the Kelvin-Helmholtz billow formation is inviscid; 2. all turbulence is formed later, by gravitational collapse of the billow; 3. turbulence length scales grow to match the large density overturn scales, and maximum ε values occur after the billow has reached its maximum vertical extent and is about 50% collapsed; 4. thereafter the vertical density overturn scales of the microstructure remain equal to the turbulence scales; and, 5. the turbulence energy scales and the microstructure overturn scales collapse together and vanish within a few Väisälä periods, independent of patch size. Gregg even suggests the possibility of billow formation and collapse without any turbulence at all. The Gregg inviscid KH billow turbulence model is described in the caption of his Figure 45:

> *"(Fig. 45 caption) Maximum overturning scales occur just before collapse. At this time ε is small but increases rapidly after collapse, assuming the collapse leads to turbulence. After collapse, both the overturning scales and ε decay in a few stability periods."*

The present analysis and interpretation of laboratory tilt tube experiments in Section 2 indicates that none of these assumptions of Gregg (1987) are correct: rather; 1. the billow formation is turbulent and it does not collapse; 2. gravitational collapse is less important at all stages than shear instability in the turbulence formation; 3. turbulence length scales are maximum when the billow size is maximum at fossilization, and ε is maximum long before this occurs; 4. after

fossilization the turbulence scales decrease but the density overturn scales do not, instead they persist as fossils without collapsing; 5. the larger the Reynolds number of the billow at the time of fossilization, the longer the microstructure fossils of the turbulence will persist, possibly for hundreds of stability periods. The application of the Gregg (1987) assumptions and the inviscid KH billow model to the interpretation of oceanic microstructure, particularly for the large density overturns of Wijesekera and Dillon (1991) and Hebert et al. (1992) is therefore questioned.

Linear stability analysis of free shear layers, with and without stratification, is reviewed by Turner (1973, Chapter 4), including photographs of the Thorpe (1968, 1971) experiments and other relevant internal wave breaking and stratified turbulence formation processes such as radar measurements of "clear air turbulence" of atmospheric "KH billows" in Turner's Fig. 4.15. As shown by Turner's Fig. 4.10, the roll size increases when the salinity interface is given sufficient time to diffuse and thicken before tilting. Figure 1ab shows the regular pattern of the eddies formed, which has been interpreted (or misinterpreted) as an inviscid, non-turbulent flow.

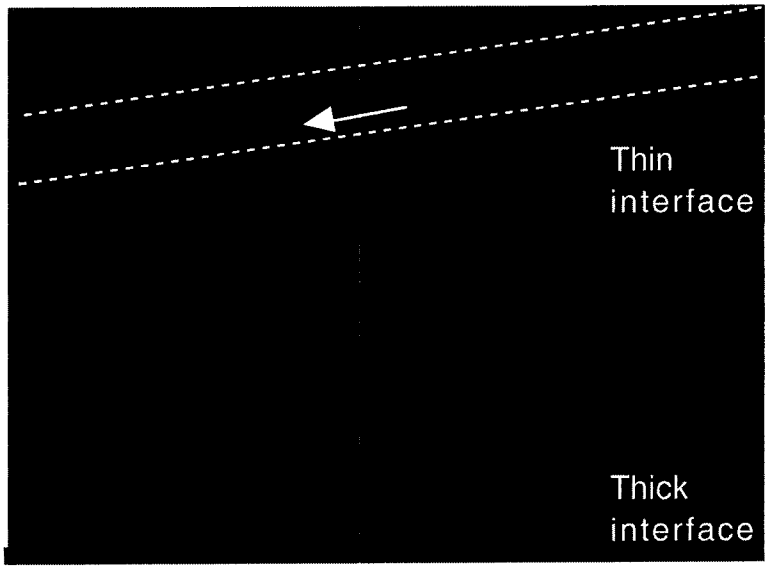

Figure 1a. From Fig. 4.10 of Turner, showing the effect of density interface thickening by three times longer diffusion time (bottom) on the size of the KH rolls and their wavelength for the Thorpe (1971) tilt tube experiments. At the top, arrows show the direction of the flow, and dashed lines show the tube walls. Are these flows inviscid? Are they turbulent? If turbulent, what is the largest scale of the turbulence?

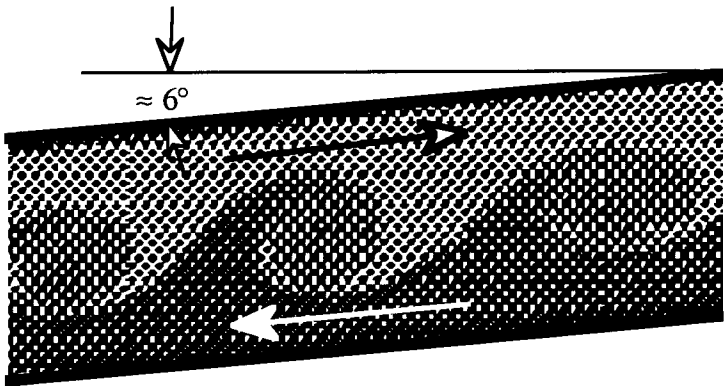

Figure 1b. Blowup of bottom flow shown in Fig. 1a. The eddies are 1.6 times larger compared to $1.7 = 3^{1/2}$ expected for 3 times longer diffusion time assuming the overturn scales are set by the density layer thickness at the initial tilt time. If the density interface is not allowed to thicken by diffusion, the overturn scale may be set by the turbulent boundary layer thickness, as described in Section 2. Flow directions caused by tilting the two density layers are shown by arrows.

Shadowgraph pictures of the density interface subjected to steady shear (achieved by tilting the tube back to horizontal at the time of roll-up) are shown in Fig. 4.12 of Turner, and appear to show the formation and final suppression of turbulence. However, Thorpe (1987) uses top view shadowgraphs to suggest that most of the turbulence shown by these side view shadowgraphs and refractive index patterns of Thorpe (1971) originates at the side walls of the tank rather than the interior of the billows. This was the interpretation used by Gregg (1987) in his inviscid KH billow model that assumes the rolls are initially nonturbulent. In addition to the side wall turbulence, the shadowgraphs revealed a complex internal structure in the roll layers, as shown in Figure 1c. Vortex tube structures can be seen, with axes in the streamwise direction of stretching, along with crosshatched patterns. From the shadowgraphs, the flow interior appears to be far from inviscid at this stage of its evolution. Thorpe (1987) sketches a set of vortex tubes within the roll with alternating vorticity aligned in the streamwise direction, which he refers to as convective instabilities. Presumably these structures originate in the boundary layers or braids with transverse vortex axes that are stretched into the streamwise direction by the roll, thus amplifying the vorticity by the $\vec{\omega} \cdot \overleftrightarrow{e}$ stretching term in the conservation of vorticity equation, where $\vec{\omega}$ is the vorticity and $\overleftrightarrow{e}$ is the rate of strain tensor.

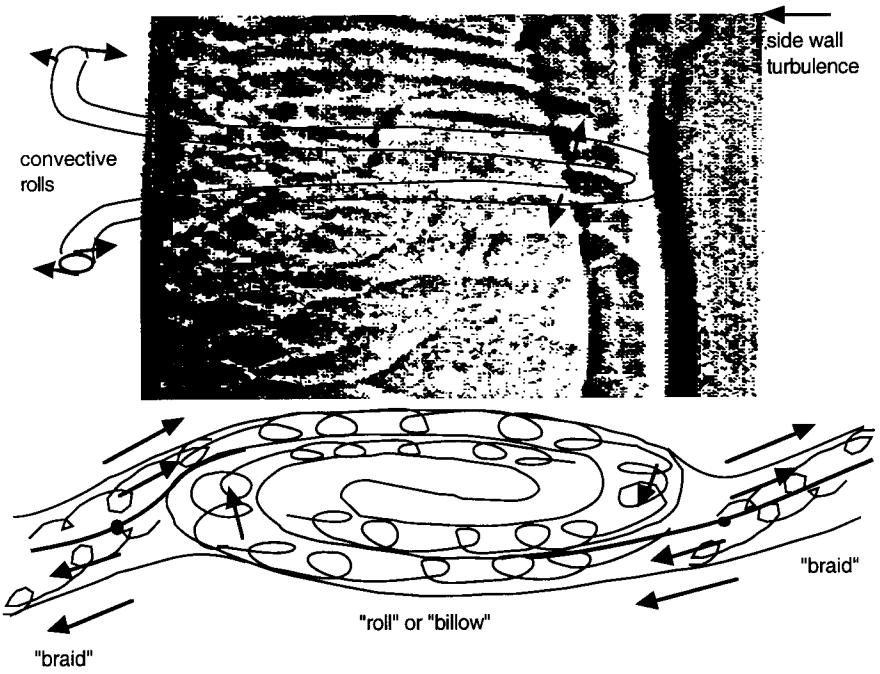

Figure 1c. Shadowgraph of top view of roll structures formed in tilt tube experiments, from Thorpe (1987, Fig. 3g), showing streamwise vortex tubes ("convective rolls") and other structures within the roll layers. The present model attributes these to vortex stretching of transverse vortices of turbulence formed in the "braid" shear layers, possibly triggered at the side walls or by interface irregularities prior to the billow formation.

In the present paper, a very different interpretation is proposed for the Thorpe tilt tube experiments, and therefore for breaking internal waves in the ocean and atmosphere, from that proposed by Gregg (1987), and assumed by Moum et al. (1989), Wijesekera and Dillon (1991), and Hebert et al. (1992) in their interpretation of ocean microstructure with large scale overturns. According to the present description of the laboratory billows, turbulence on a sheared, stratified density interface appears in four stages:

1. an inertial-viscous transition occurs (when the critical Reynolds number is exceeded) either in the two laminar boundary layers formed on opposite sides of a tilted thin density interface or in the two braids adjacent to the billow, or both, shortly before the billow forms;

2. an inertial-buoyancy transition occurs when inertial-vortex forces of the two boundary layers combine to overcome the stabilizing buoyancy forces of the density interface (the critical Froude number is exceeded); and,

3. an inertial-Coriolis transition occurs when the inertial-vortex forces of the rolled up turbulent braid boundary layers overcome the radial roll Coriolis forces (the critical Rossby number is exceeded) of the billow, leading to;

4. billow pairing and rapid growth of the fully turbulent shear layer until the turbulence energy scale is constrained by buoyancy forces at fossilization.

When the density interface is allowed to diffuse, as in Fig's. 1ab, the first turbulence transition may be delayed by buoyancy forces because the velocity and density boundary layers initially have comparable thicknesses. If so, then this diffusion thickness determines the size of the roll. However, before the roll appears, the density interface will be thinned by compressive straining in the braids. Because density interfaces in the ocean and atmosphere are always in motion, it seems likely that they will generally be thinner than vorticity interfaces; that is, universal turbulent scalar similarity hypotheses should apply, so that viscous sublayers are thicker than density sublayers by factors of $Pr^{1/2}$ or $Sc^{1/2}$, depending on whether temperature or salinity determines the density, where Pr is the Prandtl number ν/α and Sc is the Schmidt number ν/D. Figure 1d illustrates various combinations of thin and diffuse density interfaces and the expected effects on the size of the initial billow.

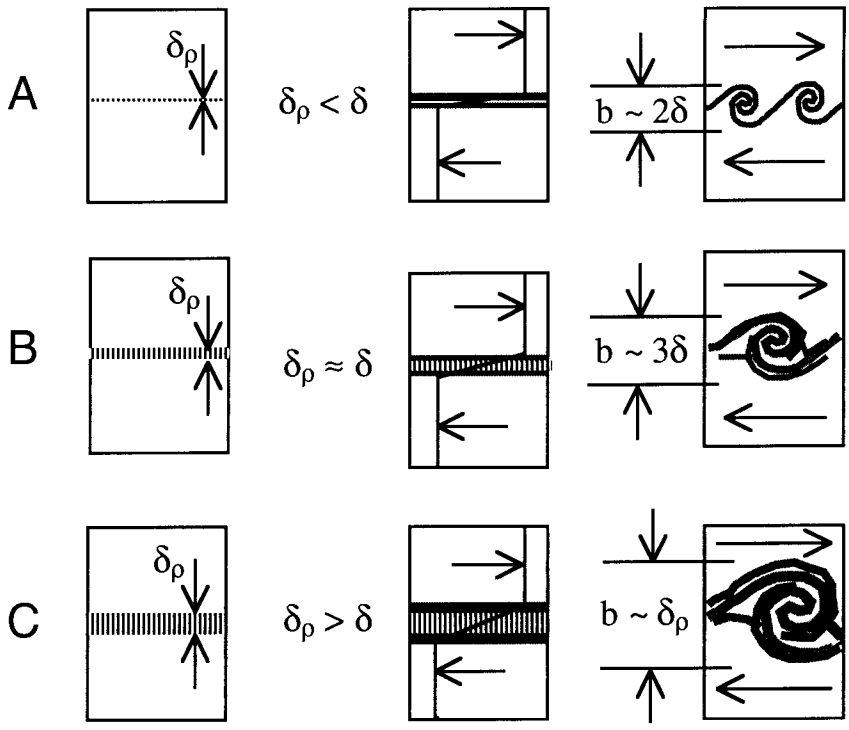

Figure 1d. Various possibilities for determining initial perturbation wavelengths λ and resulting billow sizes b on tilted density interfaces δ_ρ. In A. the interface is very thin, so the critical wavelength and billow size before pairing is determined by the thickness of the laminar or turbulent boundary layer δ, checkered line, when the Froude number first becomes critical. In C. a thick density interface, shaded line, determines the billow size. In B. a combination of boundary layer and interface thickness set the billow size.

The density interfaces in Fig. 1d are assumed to be subjected to an accelerating shear with increasing time to the right. In Fig. 1dA. the density interface δ_ρ is very thin, so the scale of the initial billow b (and its wavelength λ if more than one billow forms, where b/λ will be in a constant range of ratios of about 0.1–0.3 between the initial formation and the first pairing) is set by the

thickness of the laminar or turbulent boundary layer $\delta > \delta_\rho$ when the Froude number near the interface first becomes critical, as described below in Section 2. Fig. 1dB has interface and turbulent boundary layers of approximately equal size at the buoyant inertial billow transition. In Fig. 1dC, the density interface is thickened; for example by molecular diffusion, as in the Thorpe experiments. Other combinations are possible, such as an initially thickened velocity layer formed by combining splitter plate laminar boundary layers, as in Lawrence et al. (1991) where density and velocity interfaces are also displaced. Regular billow motions can be formed, as in the latter study, but the flow is not inviscid, and will rapidly become fully turbulent with increasing density interface thickness $\delta_\rho << L_R$ and decreasing $\varepsilon \approx U^3/\delta$ for constant U until fossilization begins when $\delta_\rho \approx L_R$. The Ozmidov scale $L_R \equiv (\varepsilon/N^3(\delta))^{1/2} \approx (U^2/g')^{3/4}\delta^{1/4}$ increases more slowly than δ_ρ before this point. Thus fossilization begins when $\delta_\rho \approx U^2/g'$, where $g' \equiv g\Delta\rho/\rho$. The inviscid length scale $\Delta \approx U^2/g'$ is discussed in Section 2.2, and appears below in equation (9).

In the ocean, a thickened density layer $\delta_\rho > \delta$, as in Fig. 1dC, could occur due to a previous turbulent shear layer, Fig. 1dA, that has diffused, thickened the density interface, and then fossilized. For example, a second tilting of the Thorpe apparatus after an initial billow experiment produces much larger billows, as in Fig. 1dC. However, if the billows in Fig. 1d A, B, and C, or any other combination, are subjected to large enough shears so that they repeatedly pair and form much larger actively turbulent shear layers, then their initial conditions will become irrelevant to the dynamics, and information about their origins will be lost. In all cases the dissipation rate ε will be larger during the actively turbulent regime when the billows first form than when they reach the maximum size permitted by the stratification and fossilization begins. Figure 1e models the qualitative behavior of ε for the Thorpe experiments, with constant velocity U after tilt back of the tube. During the initial phase, the dissipation rate in the laminar boundary layer will be $\nu(U/\delta)^2$ which decreases as the boundary layer thickness δ increases. If the boundary layer becomes turbulent, ε will increase to cU^3/δ, where c is a constant greater than $\nu/U\delta$ but less than 1. When the billow first forms, vortex lines in "braids" formed from these boundary layers (Fig. 1c) will be strongly stretched and wrapped throughout the billow. For n overturns, there are 4n +1 layers in the billow. The layers are thinned by straining, and thickened by the turbulent shear and entrainment in the braid, increasing ε to values bounded by $cU^3[4n + 1]/\delta_o$, where n is the number of overturns of the initial spinup, δ_o is the boundary layer thickness at the beginning of the spinup, and [4n + 1] is its maximum thinning factor. Spin Coriolis forces will briefly inhibit radial turbulence scales while the angular velocity U/R is large, where R is the radius of the billow. Then ε will rapidly decrease as the interior turbulence homogenizes, probably before n reaches 2. The turbulent billow continues to grow but ε rapidly decreases toward $cU^3/[4n + 1]\delta_o$ for a turbulent shear layer, where $[4n + 1]\delta_o$ is the maximum size of the billow after n overturns. Thereafter, the billows will pair, the braids will thicken further, and all information about the initial boundary layer thickness will be lost.

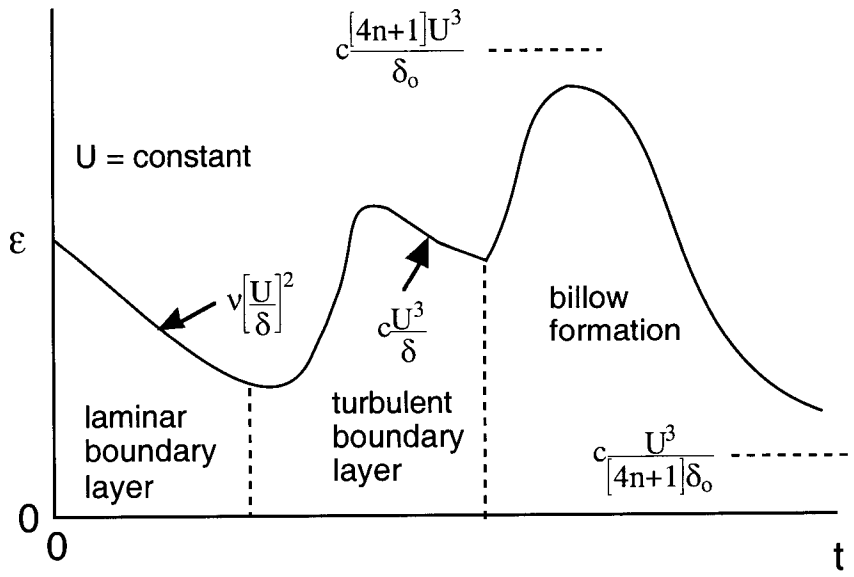

Figure 1e. Model for dissipation rate ε in Thorpe experiment boundary layers and billows as a function of time t, as described in the text. The flows are not inviscid.

2.0 Tilt tube experiments

As described by Thorpe (1968), KH billow formation on a tilted density interface was reported to the Royal Society of London by Reynolds (1883). Thorpe (1968, 1971, 1973, 1978, 1987) has explored several aspects of tilted density layers in various flows and geometries showing billow formation at the density interface. The flow illustrates a wide variety of basic turbulence processes in unstratified, stratified, and rotating fluids, as well as the stratified turbulent mixing of scalar fields with weak diffusivity such as temperature and salinity in the ocean. The present discussion is based primarily on experiments in the second author's laboratory, as shown in Fig. 1dA where the density interface is not given time to thicken by diffusion before tilting and the tube is not tilted back to horizontal before the buoyant-inertial transition. Possibly this flow is representative of tilted ocean and atmospheric density layers that are rarely quiescent or horizontal so that velocity boundary layers are generally thicker than the density interfaces on which they form. The first "wave breaking" billows for such interfaces would probably occur with accelerating rather than constant velocity shear layers. However, as discussed in Section 4, the dominant turbulent events in the stratified ocean are apparently so powerful that they must go through several eddy pairings in growth to their maximum overturning size, completely obliterating such details of their origins.

As shown in Figure 2, fresh and then dyed saline water are introduced from the bottom with the tube vertical.

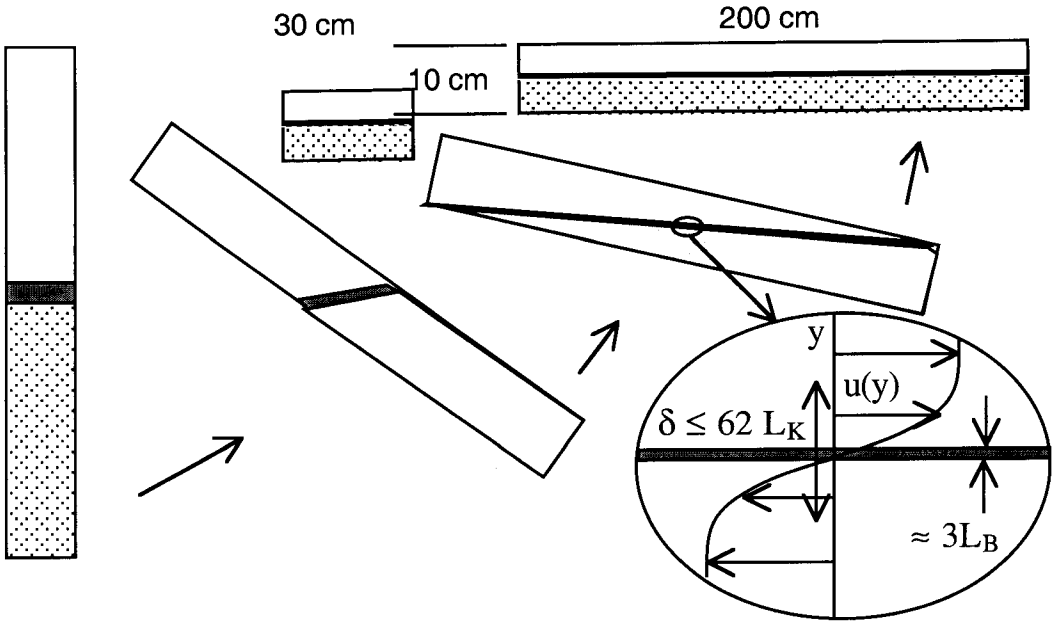

Figure 2. Setting up the tilt tube experiment. Tap water of density ρ floats over dyed salt water of density $\rho + \Delta\rho$ on the left, with a layer of intermediate density between. This intermediate density layer is compressed by the interface straining as the tube is slowly tilted to a horizontal position, keeping the viscous boundary layer thinner than $62L_K$ so it will not become turbulent. An equilibrium between convection and diffusion develops at the density interface, which cannot be made thinner than about $3L_B$. For salt, L_B is smaller than L_K by a factor of about 30, corresponding to $Sc^{1/2}$.

The tilting to horizontal in Fig. 2 is done very slowly with minimum accelerations so that the interface thins and the boundary layer flow remains laminar as the fluid within the interface layer is subjected to a uniform rate of strain γ. Without molecular diffusion the intermediate density layer would be thinned by a factor of the height to length ratio 1/20 (by the conservation of mass) for the tank, to fractions of a millimeter. Any mixing at the interface produced during the filling of the tube, forming the intermediate density fluid shown in Fig. 2, is obliterated during the tilting operation that thins the interface to a submillimeter Batchelor scale $L_B \equiv (D/\gamma)^{1/2}$ corresponding to the shear at the interface during tilting to the horizontal position shown on the right which is the initial condition. The experiment is to quickly incline the tube from an angle $\theta = 0°$ (horizontal) to $\theta \approx 4–6°$ and observe the formation of billows and turbulence near the tilted density interface. In an experiment described in the next section, a thin layer of tap water above the interface was dyed a darker color than the saline bottom layer to trace its movements.

After tilting, the two constant density slabs of fluid begin to accelerate with respect to each other in opposite directions at constant rate,

$$g'' = g(\Delta\rho/\rho)\sin\theta = g'\sin\theta, \qquad (1)$$

where $\Delta\rho$ is the density difference across the interface and g is gravity.

2.1 Boundary layer formation

The conservation of vorticity equations for stratified, incompressible, constant viscosity Newtonian fluids are

$$\frac{\partial \omega}{\partial t} + (\mathbf{v}\cdot\nabla)\omega = \omega\cdot\ \mathbf{e} + \omega\cdot\ \Omega + \frac{\nabla\rho \times \nabla p}{\rho^2} - \frac{\nabla\rho \times \nu\nabla^2\mathbf{v}}{\rho} + \nu\,\nabla^2\omega \tag{2}$$

where $\mathbf{v}$ is the velocity, $\omega \equiv \nabla \times \mathbf{v}$ is the vorticity, $\mathbf{e}$ is the rate-of-strain tensor, Ω is the rotation tensor, ρ is density, p is pressure, and ν is the kinematic viscosity. The left side of (2) is the rate of change of vorticity for a fluid particle. The right side of (2) shows that vorticity changes in magnitude and direction by stretching and rotating the vortex line of the particle, by tilting its density gradient surface from either the pressure or viscous force directions, and decreases by viscous diffusion. When the thin pycnocline in Fig. 1 is tilted, we see from (2) that shear develops only at the interface where $\nabla\rho \neq 0$, giving (1) from Stokes theorem and a time integral. Vorticity diffuses from the interface as a source, giving a boundary layer thickness δ that grows with time as

$$\delta \approx k(\nu t)^{1/2} \tag{3}$$

where the proportionality constant k is about 5 for laminar boundary layer growth on flat plates. The relation should also be valid for accelerating boundary layers, from the momentum equations, with small changes in k. Perturbations of the laminar boundary layer will be damped by viscous forces of the momentum equations

$$\frac{\partial \mathbf{v}}{\partial t} \cong -\nabla B + \mathbf{v} \times \omega + \mathbf{v} \times 2\,\Omega + \mathbf{g}' + \nabla\cdot\left(\frac{\mathbf{T}}{\rho_o}\right) \tag{4}$$

where the Bernoulli group of mechanical energy terms $B \equiv p/\rho_o + v^2/2 + gz$, the inertial-vortex force is $\mathbf{v} \times \omega$, the buoyancy force is $\mathbf{g}' \equiv [(\rho - \rho_o)/\rho_o]\,\mathbf{g}$, the inertial-Coriolis force is $\mathbf{v} \times 2\,\Omega$, the viscous force is $\nabla\cdot\ (\mathbf{T}/\rho_o)$, $\mathbf{T}$ is the viscous stress tensor, $\mathbf{g}$ is gravity, and ρ_o is the ambient density at depth z. All forces are per unit mass. The viscous stress tensor, the rate of strain tensor, and the viscous dissipation rate are related by

$$\varepsilon = 2\nu e_{ij}^2\ ;\ e_{ij} \equiv \frac{1}{2}\left[\frac{\partial v_i}{\partial x_j} + \frac{\partial v_j}{\partial x_i}\right]\ ;\ T_{ij} = 2\mu e_{ij} \tag{5}$$

Subscripts i and j are 1, 2, 3 and are summed when repeated, and μ is the dynamic viscosity. Outside the boundary layer, the only nonzero term on the right of (4) is $\mathbf{g}'$, giving (1). Within the laminar boundary layer, streamlines are parallel to the interface. Local straining perturbations are amplified by the inertial vortex force $\mathbf{v} \times \omega$ in the direction of the perturbation, but are damped by the viscous stress forces $\nabla\cdot\ (\mathbf{T}/\rho_o)$, which act in the opposite direction, as shown in Figure 3. The questions are; how thick does the boundary layer become before it becomes turbulent, and how

long does this take compared to the time required for the density interface to become unstable and form a billow?

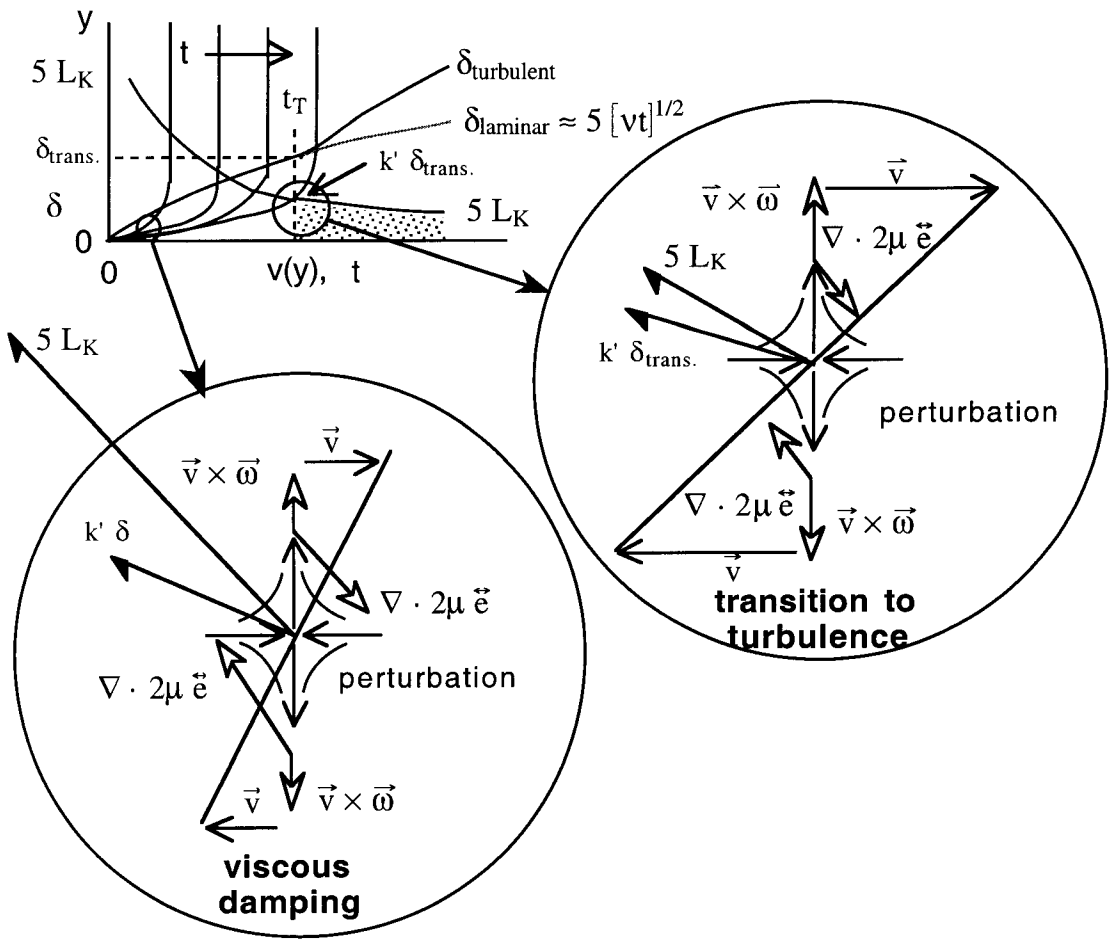

Figure 3a. Growth of the laminar boundary layers near the tilted density interface as a function of time t. For small t and δ, a straining velocity perturbation shown in the lower left circle, produces a small amplifying inertial-vortex force and a large damping viscous force. At transition k' $\delta_{tran.} \equiv 5\ L_K \approx 0.6\ \theta$, the inertial vortex forces become greater than the viscous damping forces. The viscous sublayer (dotted) of the turbulent boundary layer after transition is about 5 L_K thick.

As the boundary layer thickness δ grows with time, the ratio of the inertial-vortex to viscous forces, or Reynolds number, increases and eventually reaches a critical value beyond which perturbations grow and form the eddy-like motions of turbulence. This inertial-viscous transition to turbulence is illustrated in Fig. 3a by the equality at time t_T of the Kolmogorov length scale $L_K \equiv (\nu^3/\varepsilon)^{1/4}$, which monotonically decreases with t as ε increases, and some fraction k" of the boundary layer thickness $\delta_{trans.}$ at transition. The turbulence transition for turbulent boundary layers occurs at $y \approx 5L_K$, where ε is the wall dissipation rate so k' should be less than 5. L_K equals the wall

length $\delta^* \equiv \nu/u^*$, the friction velocity $u^* \equiv (T_{13}/\rho)^{1/2} = (\nu\varepsilon)^{1/4} \equiv U_K$, the Kolmogorov velocity, and T_{13} is the wall shear stress, and it is well known ("the law of the wall") that the viscous to turbulent boundary layer transition in a turbulent boundary layer occurs where $y \approx 5\,\delta^*$. Therefore, for comparison, define the constant $k' \equiv (5L_K/\delta_{trans.})$, where $\delta_{trans.}$ is the laminar boundary layer thickness at transition, and estimate k' and k".

The criterion given for the transition of a growing laminar boundary layer to turbulence is that the Reynolds number $Re_x \equiv Ux/\nu$ is about 4×10^5 based on the distance x from the leading edge, where U is the external velocity, White (1986, p417). Substituting (3) and $t = x/U$ into the definition of Re_x gives $Re_\delta = 5\,Re_x^{1/2}$, so $(Re_\delta)_{crit.}$ is about 3,000. Similarly, from a pipe flow transition Re_D of 2100 one can infer $(Re_\delta)_{crit.}$ of 1050, and from Re_θ at transition of 300 (Paul Libby, personal communication, 1991), $(Re_\delta)_{crit.}$ is 2200, where θ is the momentum thickness, using the von Kármán parabolic velocity profile $u/U = 2y/\delta - (y/\delta)^2$, giving $\theta/\delta = 2/15 = 0.13$. The ratio $k' \equiv (5L_K/\delta_{trans.})$ is therefore $(5/(2Re_\delta)^{1/2})_{trans.} \approx 0.08$, which is rather close to the θ/δ ratio. Thus, laminar boundary layer transition occurs when $5L_K$ decreases to $0.62\,\theta$ and $\delta_{lam.} \geq 62L_K$, giving $k'' \approx 1/62$.

Initially, L_K is large because ε is small, and decreases slowly with time as $U = g''t$ increases,

$$L_K = \left[\frac{\nu}{\left(\frac{\partial u}{\partial y}\right)_{y=0}}\right]^{1/2} \approx \left[\frac{\nu}{\frac{g''t}{\delta}}\right]^{1/2} = \left[\frac{\nu k(\nu t)^{1/2}}{g''t}\right]^{1/2} = \frac{k^{1/2}\nu^{3/4}}{g''^{1/2}}\,t^{-1/4} \tag{6}$$

proportional to $t^{-1/4}$. As indicated in (3), the boundary layer thickness δ grows with time as $k(\nu t)^{1/2}$ until transition at time t_{TS}. From (3) and the definition of Re_δ

$$t_{TS} \approx \left[\frac{(Re_\delta)_{crit.}}{k}\right]^{2/3}\left[\frac{\nu}{g''^2}\right]^{1/3} \tag{7a}$$

as shown in the upper left diagram of Fig. 3. For the thin density interface tilt tube experiments described in the next section, the inertial viscous transition from (7a) should occur at t_{TS} values of about 12 seconds compared to 10 to 16 seconds when the inertial-buoyant transition and billow roll-up occur, indicating that the boundary layers on the strong density interface may or may not become turbulent before the billow transition. Thorpe (1969) notes that the inertial-viscous (Tollmien-Schlichting) transition for his experiments in immiscible fluids may occur prior to the buoyant-inertial (Kelvin-Helmholtz) transition, and suggests his measured billow formation times should be interpreted as upper bounds. For a tilted thin density interface, substituting (3) and (5) into $Fr(y) \equiv u(y)/yN(y)$ with $y \approx \delta$ at the critical Froude number $Fr_{crit.}$ gives the time for the billow formation t_{KH} as

$$\frac{t_{KH}}{t_{TS}} \approx \frac{(kFr_{crit.})^{4/3}}{(Re_\delta)_{crit.}^{2/3}}\left(\frac{1}{\sin\theta}\right)^{2/3} \tag{7b}$$

where $k \approx 5$ and $Fr_{crit.} \approx 2$. This result is not very sensitive to the velocity profile shape, and is independent of viscosity and the interface density difference. Thus, the boundary layer may become turbulent either before or after the billow formation occurs, depending primarily on the critical Reynolds number and the angle of tilt θ. If $(Re_\delta)_{crit.}$ is 2000 the two transitions occur simultaneously for an angle of tilt of 3°, or if it is 1000 at 6°, according to (7b). The appropriate critical Reynolds number for transition on a tilted density interface is probably smaller than for smooth flat plates, especially after interface irregularities appear prior to billow formation. These will tend to trip the boundary layers, suggesting that for most of the Thorpe experiments, the boundary layer probably becomes turbulent just before or simultaneously as the billows form. For the case of a diffusively thickened density interface, the time ratio t_{KH}/t_{TS} should be increased to larger values because the Froude number of the flow near the thickened interface is $Fr = u/(d+\delta)N$, so Fr will decrease with increasing thickness d for a given time and velocity u, requiring a longer time for it to reach $Fr_{crit.}$ Therefore the velocity boundary layer will have more time to become turbulent before the KH transition and will become thicker than one for a thin interface with the same density difference and tilt angle. This behavior is shown schematically in Fig. 1d.

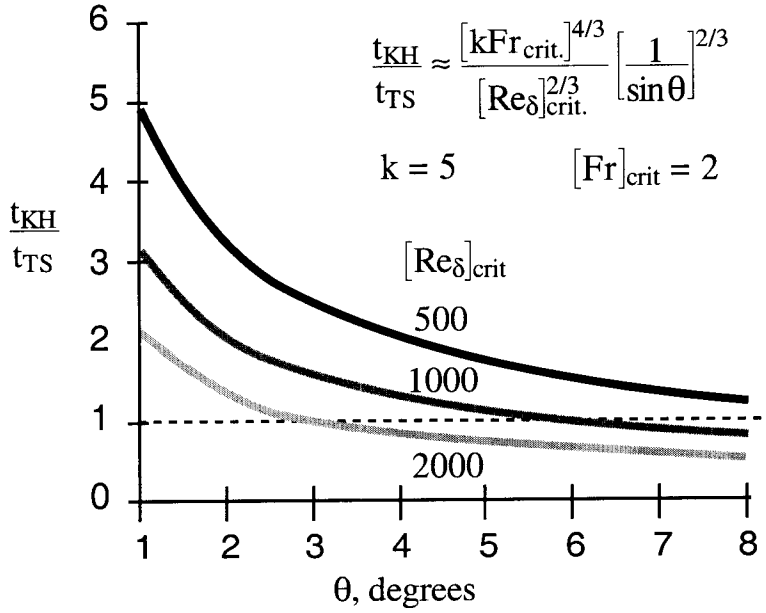

Figure 3b. Ratio of billow transition time t_{KH} to boundary layer transition time t_{TS}, from equation (7b), upper right, assuming k = 5 and $Fr_{crit.} = 2$. The smaller critical boundary layer Reynolds numbers Re_δ are probably more appropriate for the distorted interface near the billow transition time, as in Fig. 6g, indicating turbulence transition will occur prior to billow formation.

For the Thorpe (1968, 1971) experiments, the density interface diffusion thickness $\beta \approx 2\sqrt{\pi D t_{diff.}}$ controlled the size of the initial rolls, where $t_{diff.}$ is the diffusion time, as shown in Fig's. 1dC and 1a. The density gradient inhibits turbulence formation in the laminar boundary layers that form on scale β, although a turbulent boundary layer may eventually form outside this

layer as discussed above. From (2), vorticity production is not confined to the pycnocline sheet, but is distributed over a vertical distance β. Thorpe (1968) solves for the velocity as a function of the density profile in an Appendix. The conditions of the experiments reported were such that both velocity and density boundary layers changed only slightly before the critical Froude number was exceeded and KH billows would form. A similar situation occurs for laboratory mixing layer experiments, where the initial size of billows formed by the shear flows are controlled by the thickness of the boundary layers formed upstream on the flow splitter plate. The thicker the boundary layers, the larger the initial billows.

2.2. Billow formation

When the tilted density interface is initially thin, the interface thickens more slowly than the vorticity layer while the boundary layer is laminar and progressively becomes thinner in the accelerating turbulent boundary layer as the magnitude of the rate of strain $\gamma \equiv (\varepsilon/\nu)^{1/2}$ increases. If the density is caused by salinity with diffusivity D, the thickness of the interface will be about $3L_B$, where $L_B \equiv (D/\gamma)^{1/2}$. The Batchelor length scale is smaller than the Kolmogorov scale $L_K \equiv (\nu/\gamma)^{1/2}$ by a factor of about 30 because the Schmidt number $Sc \equiv (\nu/D)^{1/2}$ for salt in water is about 900. If the density difference is sufficiently large, the interface will not be disturbed because perturbations such as those in Fig. 3 are initially stabilized by buoyancy forces. The ratio of inertial-vortex forces amplifying perturbations against damping buoyancy forces is the Froude number $Fr(y) \equiv u(y)/yN(y)$, where u(y) is the streamwise velocity profile and $N(y) = (g\Delta\rho/\rho y)^{1/2}$ is the Väisälä frequency as a function of the distance from the interface y. From the definitions of Fr(y) and $g' \equiv g\Delta\rho/\rho$

$$Fr(y) = \frac{u(y)}{\sqrt{yg'}} \tag{8}$$

so for $u \sim y^n$, $n > 1/2$, Fr(y) will be zero at $y = 0$. Fr(y) approaches 0 as y approaches ∞, and will have a maximum value at $y = \delta_0$ which is some fraction of the boundary layer thickness δ, depending on the form of the velocity profile. For example, the von Kármán cubic fit to the turbulent velocity profile u(y) in (8) has maximum Fr(y) at $\delta_0 = 2\delta/3$, a parabolic fit gives $\delta_0 = \delta/3$, and a linear fit gives $\delta_0 = \delta$. The physical significance of (8) and of δ_0 is that velocity perturbations at $y = \delta_0$ are those that are most likely to cause significant perturbations to the density interface, and when $Fr(\delta_0)$ exceeds a critical value, say about 2, then the perturbations will grow and the interface will roll up. Therefore the size of the first rolls formed on the interface, and their separation wave length λ, will be proportional to δ_0 and the thickness of the turbulent boundary layer $\delta_{turbulent}$. For a turbulent boundary layer, the relevant interface Froude number will be more complex than given by (8), and will be a random three dimensional function of space and time that exceeds critical values at isolated points near the interface rather than on y surfaces (see Fig.6g and Fig. 8a below).

Once the density interface has overturned to form the system of rolls and braids, it will be rapidly scrambled by the adjacent turbulent boundary layers, as shown in Figure 4. The Froude number profile no longer has a minimum near $y = 0$, so all turbulent eddies will grow until the buoyancy forces again are able to overcome the inertial vortex forces of the turbulence, when δ equals about 0.6 times the Ozmidov length scale L_R; that is, $\delta = 0.6L_{Ro}$ at the buoyant-inertial

transition corresponding to the beginning of fossilization of the shear layer turbulence, based on fossil turbulence scale estimates summarized in Gibson (1991a).

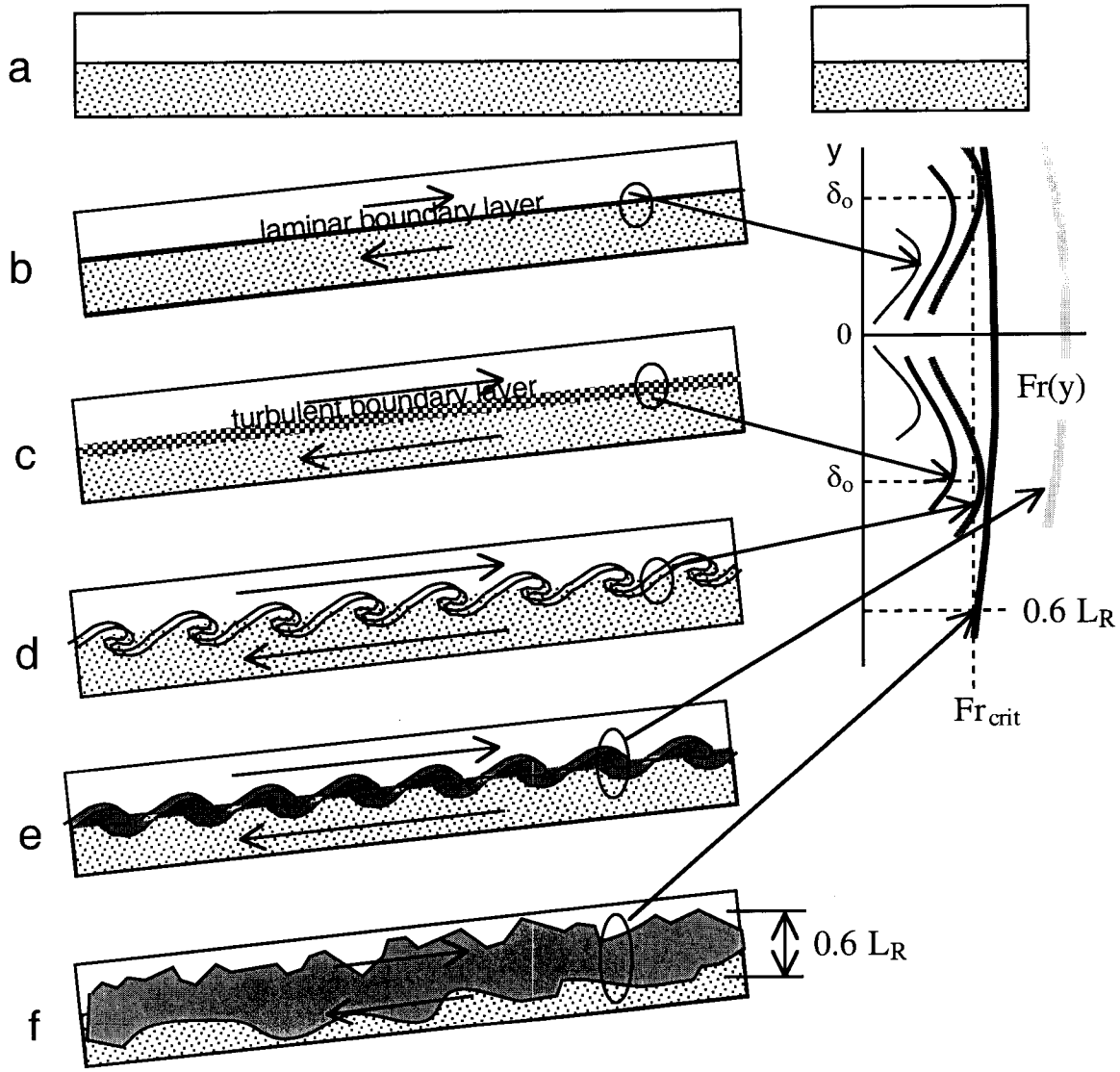

Figure 4. Formation of eddies by tilting two quiescent horizontal layers of fluid of different density, shown in **a.** The layers accelerate, forming laminar boundary layers in **b.** For small tilt angles, turbulent boundary layers of thickness δ form on both sides of the density interface in **c** as the layers accelerate. When the Froude number Fr(y) becomes critical at thickness δ_o, the turbulent boundary layers roll up into eddies of scale proportional to δ_o and the boundary layer thickness $\delta_{turbulent}$ in **d**, and the interface is mixed by the boundary layer turbulence in **e**. The eddies merge and grow to the Ozmidov scale at fossilization at **f** where the conversion of turbulence to internal waves begins, starting with the largest scales.

Effect of spin Coriolis forces on billow turbulence

During the initial roll-up of the first unstable perturbation, shown in Fig. 4d, the angular velocity of the roll (billow) will be quite large, and may inhibit turbulent motions of the braid in the radial direction due to the Coriolis force term $\mathbf{v} \times 2\,\Omega$ in (4), where Ω is the roll angular velocity. As discussed by Gibson (1991a), turbulent eddies with dissipation rate ε in a rotating flow with angular velocity Ω are inhibited from growing larger than the Hopfinger scale $L_\Omega \equiv (\varepsilon/\Omega^3)^{1/2}$ in directions perpendicular to Ω, and will form fossil two-dimensional turbulence eddies if ε decreases.

Strong spin acts on turbulence in the radial direction of the spin like strong density stratification acts on turbulence in the vertical direction, except that the fossil vorticity turbulence appears as inertial-Coriolis eddies (similar to Taylor columns) rather than internal waves, Gibson (1991d). The boundary layer turbulence dissipation rate ε in the rolls will be $c[u(\delta_0)]^3/\delta_0$ at transition, from the Kolmogorov-Obukhov law, where δ_0 is the scale at which Fr(y) first equals $Fr_{critical}$ and the constant c is < 1. The angular velocity Ω at this point will be $u(\delta_0)/\delta_0$, so substitution in the definition of L_Ω gives

$$(L_\Omega)_{trans.} = \sqrt{c}\,\delta_0 < \delta_0;\ c < 1$$

that is, the turbulence is confined by the strong spin to scales smaller than the roll layers. Therefore, initially, the turbulence in the rolls will be unable to radially scramble the embedded density interface even though it is no longer buoyancy stabilized. This seems to account for the observation from dyed flows that the density interface is preserved without mixing for a few overturnings of the rolls (see Fig. 6c below), and suggests that any assumption that the roll-up process is nonturbulent and inviscid based on this flow visualization evidence is questionable. A mathematical treatment of the analogy between density stratification and rotation is given by Vladimirov (1985).

The rolls grow with time by wrapping up fluid from the strongly sheared region between them, traditionally termed "braids". The initial braid turbulence and ε_{braid} is from those portions of the turbulent boundary layers not included in the initial rolls, and is strongly amplified by vortex stretching as the braids are rolled up forming new outer layers of the rolls. The larger the roll, the larger the braid stretching. There will also be a small increase in the accelerating external velocity, and this will also increase ε_{braid} during this short period while roll turbulence is inhibited by Coriolis forces of the roll. The enhanced braid turbulence increases the rate of entrainment of inviscid fluid and thickens the braids, and the strong turbulent stresses within the braids carries the braid fluid to the rolls. If the braids were laminar, they would be strongly thinned by compressive straining so the roll growth would be slow and require many overturns before roll pairing occurs, but this is not observed.

As the size of the spiral roll of thickening turbulent braids rapidly increases, the angular velocity $\Omega \approx u/\delta_{roll}$ eventually decreases. L_Ω increases to scales larger than the billow so the turbulence will cease to be inhibited by Coriolis forces. As this happens, the density interfaces within the rolls will be mixed away by the turbulence. This is clearly shown in the photographs (Fig. 6) of the experiment discussed in Section 2.3.1.

Development of length scales

Figure 5 shows the development of various length scales of the flow depicted in Fig. 4. After the tank is tilted the laminar boundary layer thickness δ_{lbl}, dark line, grows and $5L_K/k'$, checked line, decreases until the boundary layer becomes turbulent, point c (see Fig. 4c). Between points c and d buoyancy forces inhibit overturning of the density interface. At point d a critical Froude number Fr_{crit} is exceeded by Fr(y), and the interface, with thickness indicated by the thin line $3L_B$, overturns at the Ozmidov scale, horizontal dashes, permitting rapid growth of the turbulent "roll" and "braid" zones at e because buoyancy is unimportant at any scale. For a brief initial period while the K-H "roll" spins up, the embedded turbulence is constrained in the radial direction by Coriolis forces of the spin to the Hopfinger scale $L_{\Omega roll}$, left slant dashes, and might appear to be inviscid in flow visualizations. After billow breakup and eddy pairing, the turbulence energy scales L_O eventually grow to the Ozmidov scale upper bound $0.6\ L_R$ where they are converted to internal waves starting at f, leaving remnant fluctuations in the density field that is termed "active-fossil turbulence" while the energy scale $L_O \approx 0.6\ L_R \geq 5\ L_K$, and then becomes completely "fossil turbulence" when $L_R \leq 11 L_K$. The inviscid length scale Δ, right slant dashes, is much larger than the actual overturn scale at transition, and has no physical significance until fossilization begins at f. The microstructure and turbulence scales δ do not collapse, as assumed by the Gregg (1987) inviscid KH billow model, shown by the dark line with question marks. Gregg (1987) assumes an inviscid roll-up, with no turbulence or dissipation ε, thin line with question marks, until the roll begins gravitational collapse. The dissipation rate ε for the present turbulent KH billow model, shaded line, reaches a maximum during the initial billow roll-up, well before the maximum vertical scale has been achieved or fossilization begins at f. Values of the proportionality constants between scales were derived in the stratified turbulence theory of Gibson (1980). The experimental evidence verifying these constants is summarized by Gibson (1991a). They are uncertain by about 30%.

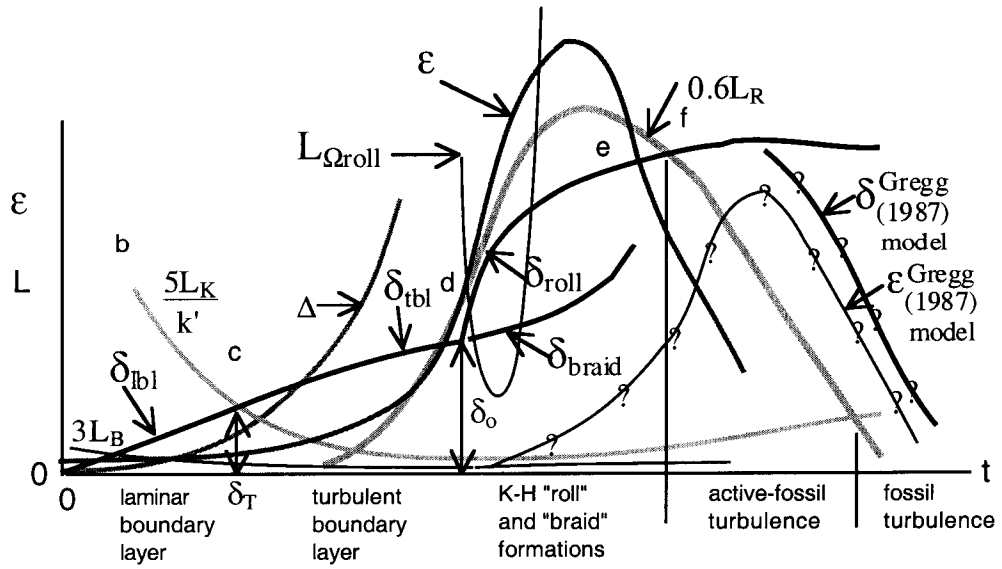

Figure 5. Schematic behavior of length scales as a function of time for the flow in Fig. 4, as described in the text. Viscous dissipation rates ε and turbulence scales δ_{tbl}, δ_{roll}, and δ_{braid} for the present turbulent KH billow model of the Thorpe experiment are

contrasted to values from the Gregg (1987) inviscid KH billow model, where the turbulence is assumed to form only in the late stages of the process due to gravitational collapse of the density overturns.

If it is assumed that the billow formation of Fig. 4 is completely inviscid, the boundary layer transition is independent of the boundary layer thickness and occurs at an initial overturn scale Δ corresponding to a critical Froude number Fr_{crit}; that is,

$$Fr_{crit}^2 = \frac{u^2}{g'\Delta} \; ; \; \Delta = \frac{u^2}{g' Fr_{crit}^2} \tag{9}$$

so Δ is initially zero and smaller than the initial boundary layer thickness δ, but will soon be much larger because Δ grows as t^2 for constant acceleration, from (9). The effect of the boundary layer is to reduce the Froude number near the interface, because $u \rightarrow 0$ as $y \rightarrow 0$, and thus delays the transition. Otherwise, transition would not be inhibited by buoyancy because the Froude number $Fr(y) = u/yN$ approaches infinity near the interface for any finite u/N ratio and roll-up would occur immediately. The size of the actual initial overturn δ is smaller than the value of Δ computed from (9) at the time of transition, as shown schematically in Fig. 5. After the interface overturns, Δ becomes proportional to the Ozmidov scale, which first increases with increasing ε from vortex stretching in the initial billow and decreasing N as the boundary layer thickness increases, and then decreases as ε decreases rapidly, but N decreases slowly. While Δ and L_R are much larger than δ, buoyancy is irrelevant to the turbulence, which is active at all scales, but when L_R decreases to about $1.6\ \delta$ the largest eddies are unable to overcome the buoyancy forces and are converted to nonpropagating, saturated internal waves, termed fossil vorticity turbulence, Gibson (1980, 1986). The remnant waves and density microstructure are forms of fossil turbulence with embedded smaller scale active turbulence. In addition, propagating internal waves may be formed in the stratified layers surrounding the active-fossil patch, termed fossil turbulence internal waves, and these may play an important roll in stratified shear layer momentum, heat, and mass transport, as well as preserving information about the previous turbulence that produced them.

2.3. Experiments

2.3.1 Dyed interface experiment

Figure 6. shows a sequence of photographs taken during a tilt tube experiment carried out at the Centre for Water Research in April, 1991. The upper layer was undyed tap water, and a small quantity of this low density layer was dyed a dark color (blue) to follow the upper boundary layer fluid. The saline (NaCl) layer below was dyed a lighter shade (red). The normalized density difference $\Delta\rho/\rho$ was about 0.011.

a. Thin density layer, tilted ≈ 6°. The acceleration g" ≈ 1.1 cm s^{-2}. The inertial-viscous transition to turbulent boundary layers on the interface should occur at t ≈ 12±4 sec from (7a), depending on $Re_{\delta crit}$.

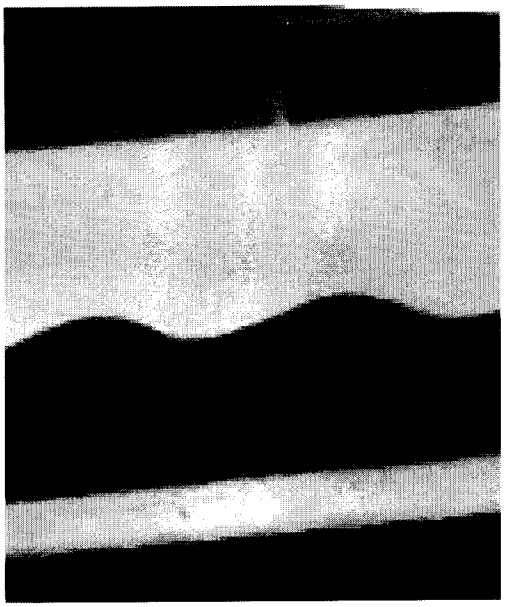

b. Near the inertial-buoyant transition after 16 seconds. The dye converges on points of growing perturbations, paired with invisible perturbations in the boundary layer below, which should now be turbulent, see 6g.

c. The billow 1.5 second after b. Note that the dye from the upper boundary layer is entirely in the billows, and is not diffusing radially, suggesting roll Coriolis constraints. Strong vortex stretching should give large ε values in the braids.

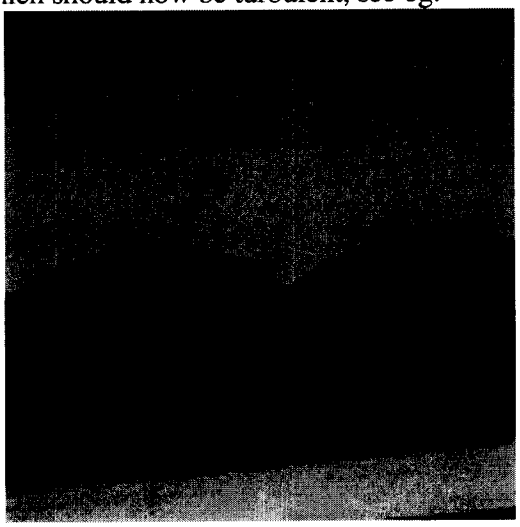

d. The turbulent boundary layers of the braids begin to scramble the organized roll structure 1.5 seconds after c, at the inertial-Coriolis transition. Dissipation rates ε and χ are probably decreasing from previous maxima but their mass integrals over the larger turbulent volume may be approaching maxima.

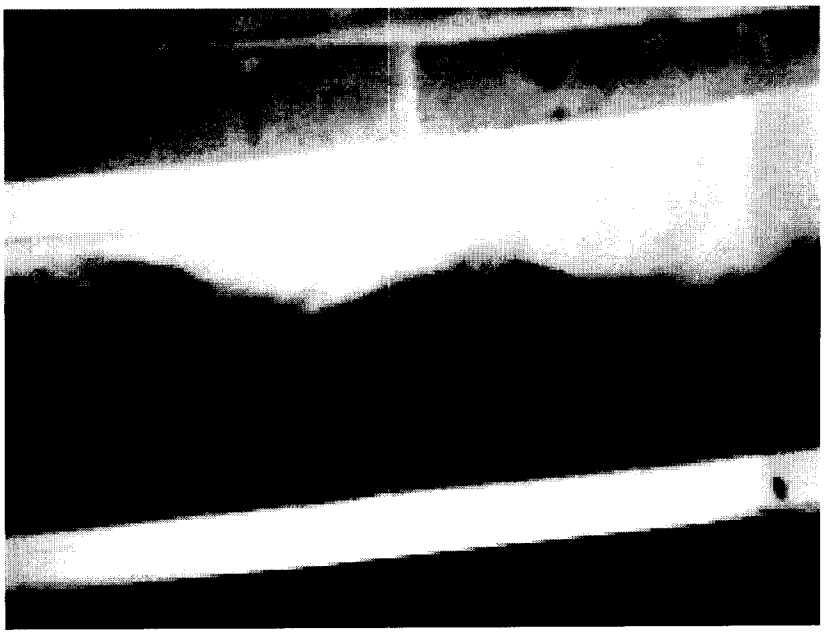

e. Fully turbulent shear layer near fossilization 1.5 seconds after d. Gravitation forces are negligible at all scales, but ε is decreasing toward ε_o at fossilization as L_T increases toward equality at this point with $0.6L_R$ which is decreasing.

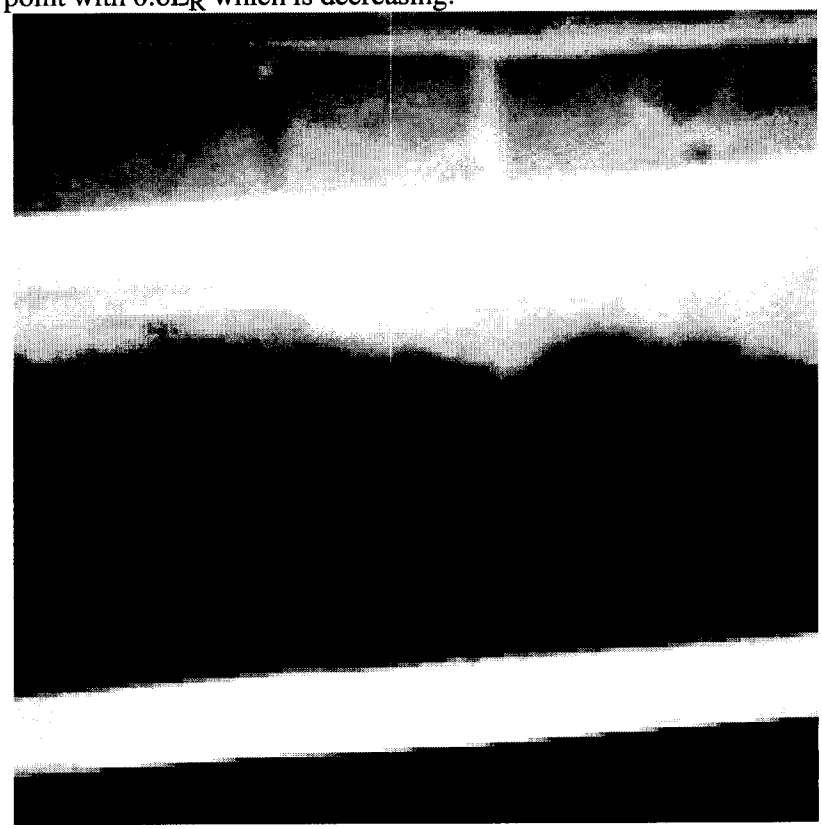

f. Active-fossil turbulence at t = 24 sec. Large scale internal waves and large overturns L_T; small L_R, small scale turbulence, and small ε. Restratification occurs but no collapse.

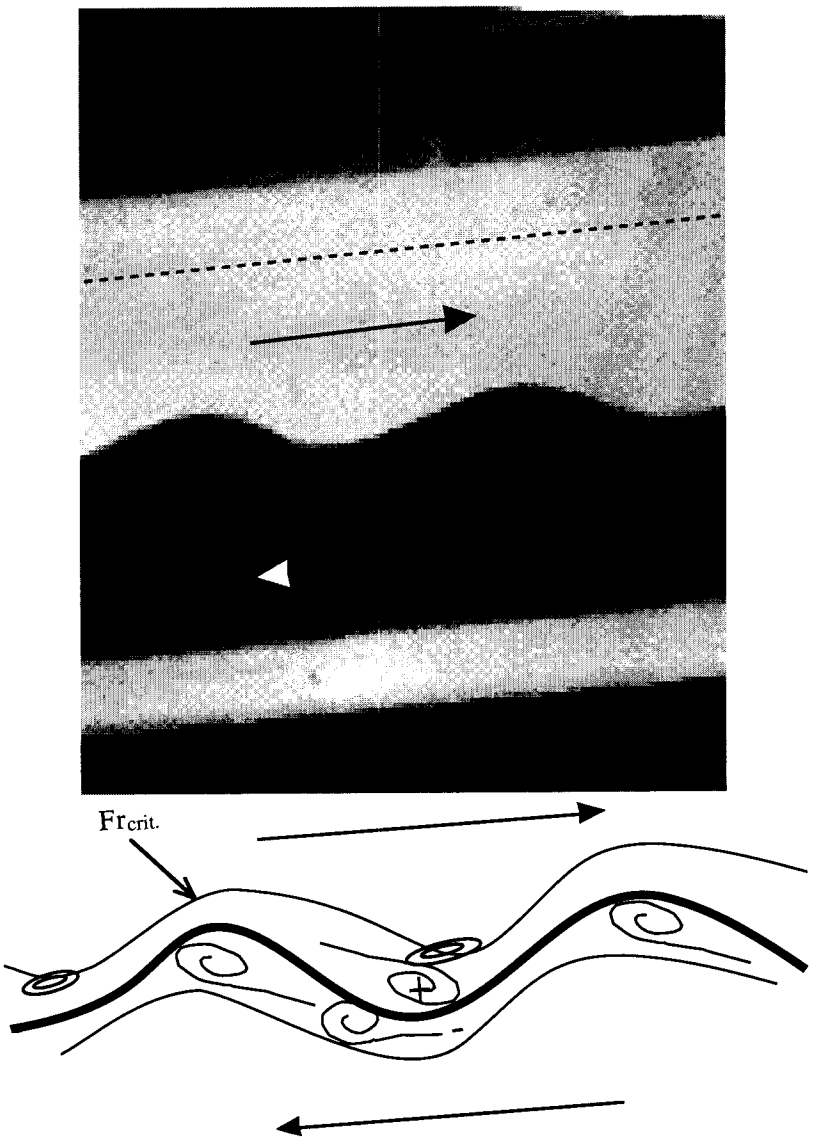

g. Model for transition in b. As the Froude number Fr(y) increases to values near $Fr_{crit.}$ in the boundary layers (which from (7a) are near inertial-viscous transition) on opposite sides of the strong density interface (dark line), finite perturbations in the interface develop and form pairs that reinforce each other. Pressure maxima (plusses) develop in the wakes of these separation points which have pressure minima (minuses). They amplify and focus the perturbations before roll-up.

Figure 6. Tilted density layer in the CWR facility, starting with a density interface less than 1 mm thick leads to a turbulent boundary layer in 12±4 seconds, from (7a), that determines the size of the billows at the buoyant-inertial transition at 16 seconds, and is shown in b. The billow growth is rapid because the braid turbulent boundary layers are thickened by turbulent entrainment of external fluid, as indicated by the dye patterns in c and d. In e and f the billows pair, forming a fully turbulent shear layer unaffected by buoyancy. A model for the transition process is shown in g.

It seems clear from the preceding discussion and the evidence of turbulence in Fig. 6 that the KH billow flow is not inviscid at any stage, and certainly not during the growth of the billow as assumed by the Gregg (1987) model. A qualitative model of ε is provided in Fig. 5, but actual measurements of the evolution ε during such flows are needed for comparison and have not been carried out. Such measurements are well within the capabilities of commercial hot film anemometers.

Even though the flows of Fig. 6, and the Thorpe tilt tube experiment of Fig. 1c and others, seem to depict turbulent rather than inviscid KH billow formation, the question remains whether some other mode of inviscid internal wave breaking may exist. Coastal plunging breakers might be taken as one precedent for inviscid internal wave breaking because these breaking waves have density overturns before the full development of turbulence on the scale or larger than the overturns. The conditions for plunging breakers involve a rapid shoaling or its equivalent in a wave current interaction, where the particle speed exceeds the phase speed of the wave and accelerations are larger than gravity. Tilt angles of pycnocline surfaces in most oceanic internal waves will usually be much less than the angles for plunging breakers.

Thorpe (1978) generated internal waves on a density interface, and imposed a shear by tilting the interface. The response of the waves was to sharpen the crests moving in the direction of the shear flow, flatten the troughs moving in the opposite direction, and damp the wave. No plunging breaker was formed, although slight breaking occurred at the sharpened crests. Figure 7 shows the observations.

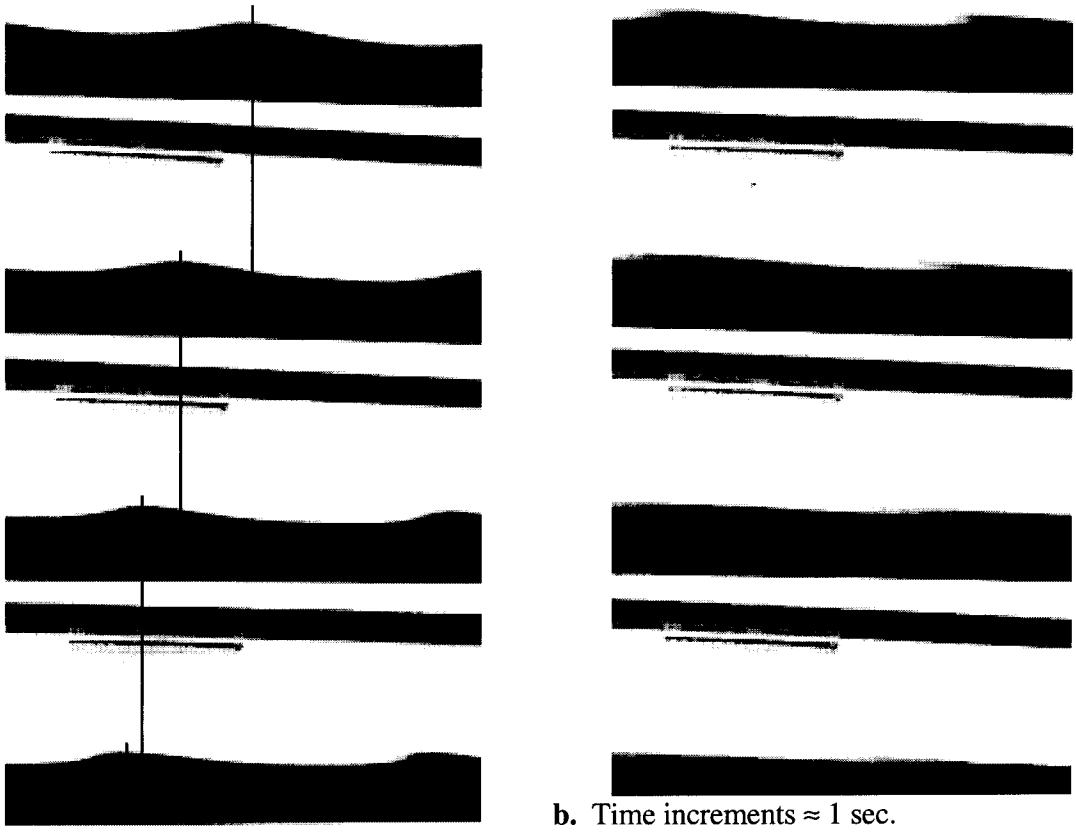

a. Time increments ≈ 1 sec, from top.

b. Time increments ≈ 1 sec.

Figure 7. Effects of shear on an internal wave, from Thorpe (1978, Fig. 9 b-e in **a.**, 9 f-i in **b.**). The wave moves to the left, top of a, as the flow accelerates in the same direction in the upper layer and opposite direction in the lower layer. The waves slow down, as shown by the vertical crest lines in a, and are damped by the shear, as shown in b. The upper crests steepen and locally break, injecting dye into the upper boundary layer where dye wisps are carried by the shear to mark the flow parallel to the interface, but no inviscid overturn is produced. The tilted density interface develops KH instabilities ≈ 1 sec after Fig. 9i at the bottom of b.

The shear interaction with the forced internal wave of Fig. 7 is similar to the interaction of very strong shear with a density interface, as obtained when the tube is tilted rapidly from a vertical to horizontal position, as shown by Thorpe (1968, Fig. 3). Powerful turbulent boundary layers fill the tube, and form cusped "breaking waves" on the dyed intermediate density fluid floating on the strong density interface, but the strong interface is flattened by the shear. The wisps of dye show the presence of large eddies in the boundary layer, and the cusps presumably reflect the locations of boundary layer separation points and $Fr_{crit.}$ points where locally segments of the density interface are torn away, just as the dye wisps emitted from wave crests in Fig. 7 presumably represent such

localized interface breakdown. Figure 8 shows the cusped waves of Thorpe (1968, Fig. 3) and a model for such events.

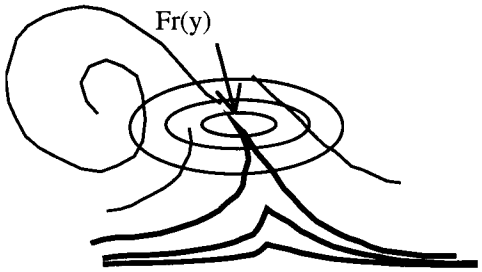

a. In strongly turbulent boundary layer, points with supercritical Froude numbers may develop near stagnation points that can locally break the density interface (dark lines at different times).

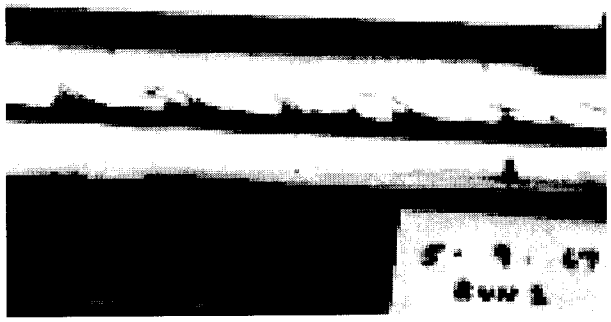

b. Formation of cusped waves in tilt tube experiment with large, rapid tilting, forming strong turbulence in shear layers. Critical Fr points such as those shown in a. form over the intermediate density layer, but not below the strong layer.

Figure 8. a. Model for cusped wave breaking. **b.** From Thorpe (1968, Fig. 3a). Strong turbulence in the upper shear layer tears away wisps of dyed intermediate density fluid, locally breaking the upper density interface. The stronger lower density interface is flattened, as in Fig. 7, but no KH billows form. At a later stage stronger turbulence in the lower layer begins to tear away wisps of dye from the lower interface as well, Thorpe (1968, Fig. 3b).

According to the present model, for very strong shear flows and thick turbulent boundary layers on weak density interfaces, Fig. 8ab, the interface is broken by many turbulent stagnation points of the boundary layer flow, where $Fr(y) \geq Fr_{crit.}$ locally, and the scale of the cusps reflect the distance from the interface where this occurs. Clearly, for turbulent boundary layers, the relevant Froude number for interface breaking is a random function of space and time, and might be indicated more precisely as $Fr(\mathbf{x},t) \equiv v(\mathbf{x}, t)/yN(\mathbf{x}, t)$ rather than Fr(y), where v is the y component of the perturbation velocity a distance y normal to the surface. Lawrence et al. (1991, Fig.'s 5, 6 and 7) apparently produce cusped wave breaking in a flow with a thick viscous boundary layer emerging at higher speed over a thin density interface. Regular eddy tubes form in the upper layer that are able to break the interface and form cusps of dye from the dense lower layer, presumably at critical Fr(y) points (lines) over the interface as shown in Fig. 8a.

To summarize, the available laboratory experiments show no evidence of any inviscid internal wave breaking modes. Viscous dissipation rates appear to be large at the early rather than later stages and the billows that form are turbulent. For small tilt tube angles, strong density interfaces are not broken by the boundary layer flow, either turbulent or laminar, because the interface Froude number Fr(y) is subcritical for small shears and reaches a maximum value at finite

distances y from sharp interfaces less than the thickness of the boundary layer δ. The size of KH billows observed reflect the thickness δ because the distance δ_0 from the interface where Fr(y) first becomes greater than $Fr_{crit.}$ occurs near $y \approx \delta$, as shown in Fig. 6.g. This thickness can be increased initially by allowing the density interface to diffuse, causing an earlier inertial-buoyancy transition, as in Fig. 1a. The braids and billows formed are strongly turbulent throughout their development, with maximum dissipation rates occurring at times prior to the beginning of fossilization of the largest turbulent eddies of the turbulent shear layer.

For accelerating shear interacting with forced internal waves, Fig. 7, the stronger shears slow and flatten the waves, sharpen crests moving in the shear flow direction, and locally break the density interface at separation points with $Fr(y) \geq Fr_{crit.}$ near the crests. For uniform stratification N, the maximum amplitude $y_{max.}$ of an internal wave moving in a uniform shear layer S is determined by the distance y from the wave central layer where the shear velocity equals the wave velocity. The wave velocity c will be of order $N(y\lambda)^{1/2}$ and the shear velocity will be of order Sy, where λ is the wavelength of the wave and S is the shear, so that

$$y_{max.} \approx (N/S)^2\lambda.$$

For a given wavelength in an accelerating shear, the maximum possible amplitude rapidly decreases as the shear increases. Thus, for a constant shear layer, small scale internal waves cannot develop with large amplitude without breaking.

3. Conclusions

Observations and analysis of tilt tube experiments support a turbulent Kelvin-Helmholtz billow model for stratified turbulence in the laboratory, ocean, or atmosphere, and do not support inviscid KH billow or internal wave breaking models such as in Gregg (1987), that are used to interpret microstructure patches with large density overturns but small ε in the Pacific equatorial undercurrent as waves that are breaking but not yet fully turbulent, Wijesekera and Dillon (1991) and Hebert et al. (1992). Such patches are reinterpreted by Gibson (1991c) as fossil turbulence remnants of powerful previous turbulence events that have produced the internal wave packets in which they are embedded, and may dominate the vertical transport processes in the undercurrent.

Analysis of the stability of the boundary layers that form on a thin, tilted, density interface predict the dependence of inertial-viscous and buoyant-inertial transition times on the density difference, the tilt angle, and critical Reynolds and Froude numbers in equations (7a) and (7b). Laboratory experiments show evidence, supporting (7b), of turbulent boundary layer formation simultaneously or just prior to billow formation, with the initial billow scale determined by the boundary layer thickness and a critical Froude number being exceeded at a finite distance from the density interface that determines the initial scale of the billow. Billows formed from density interfaces thickened by previous molecular or turbulent diffusion, such as Thorpe (1971), or by combining boundary layers from splitter plates, such as described by Ho and Huerre (1984), may form larger initial billows. However, the billow and braid structures in these flows should also soon develop into fully active turbulence "braid" shear layers independent of buoyancy forces or the initial conditions.

The well organized structure observed from dye patterns in the initial billow formation despite strong turbulence may be briefly preserved by radial Coriolis forces in the billow during its

rapid roll-up. This organized appearance may contribute to the widely held perception, presumably a misconception, that such KH billow formation is virtually inviscid, and that KH billows in the atmosphere and ocean may also be inviscid. Shadowgraph photographs of Thorpe (1987) and others have shown clear evidence of "secondary instabilities" that may be strong turbulence in this initial phase, rather than inviscid flow. Direct measurements of dissipation rates and the internal structure of these laboratory flows are unavailable and should be carried out in future experiments with high priority.

Acknowledgments

The first author is grateful to Jim Moum and Tom Dillon for supplying preprints and data reports for their papers on the TROPIC HEAT large overturn events as well as interesting discussions about possible interpretations of the data. Several colleagues have contributed to the development of the ideas presented here, particularly Charles Lemckert of the CWR who organized the tilt tube experiment demonstrations described in the paper during July 1990 and April 1991 visits to UWA, and David Luketina, who participated in lively discussions of the results. His research support was supplied by NSF and ONR, and travel to Australia by the CWR. Professor Steven A. Thorpe provided numerous excellent suggestions and detailed comments on early versions of the manuscript.

References

Artemyeva, T. S., I. D. Lozovatskiy and V. N. Nabatov, Turbulence generation in the core of the Lomonosov Current in the vicinity of local frontal zones, *Oceanology, 29*, 41-48, 1989.

Baker, M. A. & Gibson, C. H., Sampling turbulence in the stratified ocean: Statistical consequences of strong intermittency, *J. of Phys. Oceanogr., 17*, 1817-1837, 1987.

Gibson, C. H., Fossil temperature, salinity, and vorticity turbulence in the ocean, in *Marine Turbulence*, J. Nihoul (Ed.), Elsevier Publishing Co., Amsterdam, 221-257, 1980.

Gibson, C. H., Internal waves, fossil turbulence, and composite ocean microstructure spectra, *J. Fluid Mech. 168*, 89-117, 1986.

Gibson, C. H., Oceanic turbulence; big bangs and continuous creation, *J. Physicochem. Hydrodyn. 8 (1)*, 1-22, 1987a.

Gibson, C. H., Fossil turbulence and intermittency in sampling oceanic mixing processes, *J. Geophys. Res. 92(C5)*, 5383-5404, 1987b.

Gibson, C. H., Turbulence, Mixing and Microstructure, in *Ocean Engineering Science: The Sea-Vol. 9, Part A*, Edited by Bernard Le Mahaute and D. M. Hanes, Wiley Interscience, New York, 631-659, 1990.

Gibson, C. H., Laboratory, numerical, and oceanic fossil turbulence in rotating and stratified flows. *J. Geophys. Res.*, 96 (C7), 12,549-12,566, 1991a.

Gibson, C. H., Kolmogorov similarity hypotheses for scalar fields: Sampling intermittent turbulent mixing in the ocean and galaxy. *Turbulence and stochastic processes: Kolmogorov's ideas 50 years on, Proc. Roy. Soc. Lond. A, 433 (no. 1890)*, 149-164, 1991b.

Gibson, C. H., Turbulence, mixing, and heat flux in the ocean main thermocline, *J. Geophys. Res.*, 96 (C11), 20,403-20,420, 1991c.

Gibson, C. H., Fossil two-dimensional turbulence in the ocean. In *Turbulent Shear Flows, 7*, edited by F. Durst and W. C. Reynolds, Springer-Verlag, Berlin, 63–78, 1991d.

Gibson, C. H., Turbulence, in Encyclopedia of Physics, R. G. Lerner and G. L. Trigg (Eds.), Addison-Wesley Publishing Co., Inc., 1310-1314, 1991e.

Gregg, M. C., Diapycnal mixing in the thermocline: A review, *J. Geophys. Res., 92(C5)*, 5249-5286, 1987.

Hebert, D., J. N. Moum, C. A. Paulson, and D. R. Caldwell, Turbulence from internal waves at the equator, Part II: Details of a single event. *J. Phys. Oceanogr., 22, 11,* 1346-1356, 1992.

Ho, C. M. and P. Huerre, Perturbed free shear layers, Ann. Rev. Fluid Mech., 16, 365-424, 1984.

Imberger, J. and G. Ivey, On the nature of turbulence in a stratified fluid. Part 2: Application to lakes, *J. Phys. Oceanogr.*, in press, 1991.

Lawrence, G. A., F. K. Browand and L. G. Redikopp, The Stability of a sheared density interface. *Phys. Fluids A 3 (10)*, 2360–2370, 1991.

Lumley, J. L., Some comments on turbulence. *Physics of Fluids A, 4, (2)*, 203-211, 1992.

Moum, J. N., D. R. Caldwell, and C. A. Paulson, Mixing in the equatorial surface layer and thermocline, *J. Geophys. Res., 94*, 2005–2021, 1989.

Moum, J. N., D. Hebert, C. A. Paulson, and D. R. Caldwell, Turbulence from internal waves at the equator, Part I: Statistics. *J. Phys. Oceanogr., 22, 11,* 1330-1345, 1992.

Reynolds, Osborne, An experimental investigation of the circumstances which determine whether the motion of water shall be direct or sinuous, and of the law of resistance in parallel channels. *Phil. Trans and Scientific Papers, vol. 2,* 1883.

Rosenhead, L., The formation of vortices from a surface of discontinuity. *Proc. Roy. Soc.* A *134*, 92–170, 1931.

Thorpe, S. A., A method of producing a shear flow in a stratified fluid. *J. Fluid Mech. 32,* 731-751, 1968.

Thorpe, S. A., Experiments on the instability of stratified shear flows: immiscible fluids. *J. Fluid Mech. 39,* 25-48, 1969.

Thorpe, S. A., Experiments on the instability of stratified shear flows: miscible fluids. *J. Fluid Mech. 46,* 299-319, 1971.

Thorpe, S. A., Experiments on instability and turbulence in a stratified shear flow. *J. Fluid Mech. 61,* 731-751, 1973.

Thorpe, S. A., On the shape and breaking of finite amplitude internal gravity waves in a shear flow. *J. Fluid Mech. 85,* 7-31, 1978.

Thorpe, S. A., Transitional phenomena and the development of turbulence in stratified fluids: A review. *J. Geophys. Res., 92,* 5231-5248, 1987.

Turner, J. S., Buoyancy Effects in Fluids, Cambridge University Press, Cambridge, London, 1973.

Van Dyke, M., An album of fluid motion. The Parabolic Press, Stanford, California, 1982.

Vladimirov, V. A., Example of the equivalence of density stratification and rotation. *Dokl. Akad Nauk SSSR 284,* 310-313, Sept. 1985 (Trans. Sov. Phys. Dokl. 30(9), Sept. 1985).

Wijesekera, H. W. and T. M. Dillon, Internal waves and mixing in the upper equatorial Pacific ocean, *J. Geophys. Res., 96(C4)*, 7115–7125, 1991.

White, F. M., *Fluid Mechanics, 2nd Ed.,* McGraw-Hill, New York, 1986.